

Thermal Stability Analysis and Design for Electrical Product in Short-Circuit Fault

Jing Hao¹, Jungang Zhou^{2,3,*}, Yachao Wang¹

¹*School of Information Technology, Hebei University of Economics and Business, No. 47, Xuefu Road, Shijiazhuang, Hebei, China*

²*School of Electrical Engineering, Hebei University of Technology, No. 5340, Xiping Road, Beichen District, Tianjin, China*

³*Shandong Institute for Product Quality Inspection, No. 31000, Jingshi East Road, Jinan, Shandong, China*
jungang1983@126.com

Abstract—In short-circuit faults, the thermal stability of the metal conductor is an important factor for electrical products, which directly affects the safe use of the products. Because it is dangerous to test the thermal stability under short circuit, it is difficult to obtain the required power supply in a conventional laboratory, so at present, the research on thermal stability is mostly based on the theoretical analysis of the finite element method. In this paper, a short-circuit fault is studied. The short-time withstand current test is adopted, in which the current and time can be controlled. First, the results compare three formulas for calculating the current density and verify them. The temperature and current variation of the conductor are calculated and tested. The theoretical results are compared with the experimental results, and the current variation model I is established. Then, the short-time withstand current test is carried out to verify the theoretical calculation, and model II is designed, which is a modification of model I. Finally, a product design method is proposed and verified by experiments. This basic research is the verification test of the theoretical literature, and the research results can be applied to the design of electrical products under short-circuit fault.

Index Terms—Short-circuit fault; Metal conductor; Electrical product design; Thermal stability; Short-time withstand current test.

I. INTRODUCTION

When a short-circuit fault occurs in an electrical product, the short-circuit current I_k through the metal conductor can be several or even hundreds of times greater than the rated current. The current I_k can generate a considerable amount of heat in the metal conductor in a short period of time. The thermal stability of the electrical product may be compromised, consequently. Thermal stability is an important factor leading to electrical aging. Therefore, it is necessary to study the thermal stability of the metal conductor in short-circuit fault, which is of very important guiding significance for the design of electrical products.

Because it is dangerous to test the thermal stability under

short circuit, it is difficult to obtain the required power supply in a conventional laboratory. To date, the finite element method (FEM) has been used to simulate the thermal stability of complex products in short-circuit tests. In some product studies, FEM has been used to simulate the mechanical properties and temperature field of a product. Under steady and short-circuit conditions, Ding, Zhu, Le, Zhang, Bao, and Cui [1] developed a 3D coupled field FEM model to analyze the electrical, thermal, and mechanical properties of a plug-in connector. In [2], the finite element method was applied to create faulty scenarios, and commercial software (Flux2D) was used to simulate the electromagnetic and thermal behavior of the machine for various degrees of severity of the aforementioned faulty modes. Staliulionis, Zhang, Pittini, Andersen, Noreika, and Tarvydas [3] proposed a thermal modelling which used the COMSOL finite element analysis software and measured the thermal field distribution. Qi, Zafarani, Akin, and Fedigan [4] performed a 2D FEM simulation and an experimental test to diagnose a short-circuit fault for permanent magnet synchronous machines and compared the DC current for different system states, such as healthy, eccentricity fault, and short-circuit fault. Gbégbé, Rouached, Cros, Bergeron, and Viarouge [5] developed a model that combines magnetostatic FEM with a coupled circuit model under a sudden three-phase short-circuit and validated the model by simulations and experiments with a 109-MVA hydrogenerator.

At present, thermal stability is usually studied by simulating a short-circuit fault. Yang, Xiong, He, and Chen [6] used the random forest model to develop an effective classification method to detect electrolyte leakage and proposed a three-step model to identify an external short-circuit fault. In [7], the thermal runaway response due to a short circuit in a prismatic lithium iron phosphate battery is investigated, the initial simulation temperature, the applied heat transfer coefficient, and the fraction of the void of the electrode have a large effect on the thermal runaway response. In [8], the influence of temperature on the stability of current sources in static and dynamic operating states was analyzed. Hossam-Eldin, Lotfy, Elgamel, and Ebeed [9] used a short-circuit DC fault identifier, a single current sensor, and

Manuscript received 30 July, 2021; accepted 29 March, 2022.

This research was supported by Research Foundation of Hebei University of Economics and Business under Grants No. 2019YB08 and No. 2019YB11; Science and Technology Research Youth Fund of Colleges and Universities of Hebei Province under Grant No. QN2022061.

inherent traveling waves to accurately identify the short-fault location and pole in multiple cables in a multiterminal high-voltage DC system. In [10], superconducting fault current limiters were applied to a power network for coordinated instantaneous overcurrent protection. It was found that it is difficult or sometimes impossible to simultaneously ensure selectivity and sensitivity. Hrbac, Kolar, Bartłomiejczyk, Mlcak, Orsag, and Vanc [11] described the effect of temperature on the thermal stability of the voltage divider. In [12], experiments were carried out on three different silicon carbides under short-circuit conditions and design guidelines for short-circuit protection were proposed to improve the reliability and availability of the entire system. In [13], the authors present a novel short-circuit test method for a distribution transformer based on an energy storage short-circuit test device, which can complete the short-circuit field test for a distribution transformer. However, most of the research results remain in the theoretical analysis stage. Due to the limitations of the power supply capacity and test equipment, the short-circuit fault test has not been fully demonstrated, which cannot provide a reliable basis for product design.

The short-time withstand current test is used to assess the thermal effect of electrical products bearing a short-circuit fault current within the specified time, which is called the “thermal stability process of the short-time withstand current test”. For the research of the short-time rated withstand current, ANSYS software is generally used to model, analyze, and simulate the parameters in the test process [14]–[16].

In this paper, we perform theoretical calculations and verification for a short-time withstand current test. Considering the test as an adiabatic process [17], [18], we introduce two equations to calculate the current density. We derive the current density equation using electrical engineering design principles. The above-mentioned equations are used to calculate the temperature of a copper conductor, and the differences in the results are discussed. The first equation applies to an adiabatic process, and the second equation is derived using the Wiedemann-Franz law. We compare the results for the temperature of the copper obtained using the two above-mentioned equations to prove that the first equation is valid under the Wiedemann-Franz law. Variations in current and resistance are calculated for different current densities and current times, and the results are discussed. The above-mentioned theoretical calculation and analysis are used to verify the current change model. Next, we perform a short-time withstand current test, whereby the current change model I is modified to produce the current change model II. We propose the product design steps and perform a test to verify model II. The copper conductor that is used in the short-time withstand current test consists of a single core polyvinyl chloride (PVC) copper conductor and a knife switch copper conductor. The verification test shows that the capacity of the test system is sufficiently large. The LDS Genesis Tower data collection system [19] (LDS) is used to collect the test current waveforms. The parameters of the current waveforms are varied to determine the change rules and establish a mathematical model. This research study provides guidelines

for the design of electrical products and can be applied to short-circuit faults.

This paper is organized as follows. The current density calculation methods are presented and compared in Section II. The conductor temperature and current changes are presented and compared in Section III. The short-time withstand current tests are presented in Section IV. The electrical product design method is proposed in Section V. Conclusions are drawn in Section VI.

II. CURRENT DENSITY CALCULATION

A. Current Density Equation

The parameters of the current density equation are listed in Table I.

TABLE I. PARAMETER LIST.

Symbol	Quantity	Unit
J_k	Current density	A/m ²
I_k	Short-circuit current	A
l	Conductor length	m
S	Conductor cross-sectional area	m ²
r	Density	kg/m ³
c	Specific heat	J/(kg · °C)
ρ_0	Resistivity at 0 °C	Ω · m
α	Resistance temperature coefficient	1/°C
t_k	Current time	s
θ_k	Conductor final temperature	°C
θ_0	Conductor initial temperature	°C
K_f	AC additional loss coefficient	Empirical value
Q_d	Thermal effect of current	A ² s
K	Constant	522×10^6 (W · s/(Ω · cm ⁴)) for copper
τ	Constant	235 °C for copper
L	Lorenz constant	2.4×10^{-8} V ² /K ²
λ	Thermal conductivity	$\lambda = 401$ W/mK for copper
T	Absolute temperature	K

In a short-circuit fault, the heat generated by the current cannot be emitted, corresponding to an adiabatic process [20]. The current density is calculated using (1) [21]

$$J_k = \frac{I_k}{S} = \sqrt{\frac{rc}{\rho_0 \alpha t_k} \ln\left(\frac{1 + \alpha \theta_k}{1 + \alpha \theta_0}\right)}. \quad (1)$$

For an AC current flowing through the conductor, an additional AC loss coefficient K_f must be added to (1) to account for the current skin effect and the proximity effect, as in (2) [22]

$$J_k = \frac{I_k}{S} = \sqrt{\frac{rc}{K_f \rho_0 \alpha t_k} \ln\left(\frac{1 + \alpha \theta_k}{1 + \alpha \theta_0}\right)}. \quad (2)$$

As accurate values for K_f are not available, K_f is selected from [22]. The uncertainty in the estimation of this parameter places a limitation on the use of (2) to calculate J_k under different conditions.

B. Derivation of Current Density Equation

An increase in the conductor temperature softens the conductor material and decreases the strength of the material.

This deterioration affects the safe use of an electrical product. Different conductor materials have different specified θ_k values. For example, a copper conductor has a θ_k value of 300 °C.

The thermal stability of a short-circuit fault is considered in electrical engineering design, and the corresponding design equation is given in (3) [23]

$$S \geq \frac{\sqrt{Q_d}}{C}. \quad (3)$$

Equation (3) can be rearranged to obtain (4)

$$C \geq \frac{\sqrt{Q_d}}{S}. \quad (4)$$

Using $Q_d = I_k^2 t_k$ yields

$$C \geq \frac{\sqrt{I_k^2 t_k}}{S} = \frac{I_k \sqrt{t_k}}{S} = J_k \sqrt{t_k}, \quad (5)$$

where $C = \sqrt{K \ln \frac{\tau + \theta_k}{\tau + \theta_0} \times 10^{-4}}$.

Then

$$J_k \leq \sqrt{\frac{K}{t_k} \ln \frac{\tau + \theta_k}{\tau + \theta_0} \times 10^{-4}}. \quad (6)$$

For $t_k = 1$ s,

$$J_k \leq \sqrt{K \ln \frac{\tau + \theta_k}{\tau + \theta_0} \times 10^{-4}}. \quad (7)$$

For convenience of calculation, the maximum value of the thermal stability is used

$$J_k = \sqrt{K \ln \frac{\tau + \theta_k}{\tau + \theta_0} \times 10^{-4}}. \quad (8)$$

Equation (8) can be used to calculate the current density, where K is a material-dependent constant, and compared to IEC standard 60949 [24], the current density is roughly the same.

C. Calculation Comparison

Example 1. As an example, a copper conductor is selected, where $r = 8.9 \times 10^3$ kg/m³, $c = 0.39 \times 10^3$ J/(kg · °C), $\rho_0 = 1.67 \times 10^{-8}$ Ω·m, $\alpha = 0.0039$ (1/°C), $t_k = 1$ s, $\theta_0 = 20$ °C, and $\theta_k = 300$ °C.

Substituting these values into (1) yields $J_{k1} = 193.1$ A/mm².

Substituting the value of K_f in (2) yields $J_{k2} = 152$ A/mm².

Using (8) yields $J_{k3} = 196.7$ A/mm².

Comparing the values of J_{k1} , J_{k2} , and J_{k3} shows that J_{k1} and J_{k3} are almost equal and larger than J_{k2} . Thus, (1) and (8) have different forms but yield almost equal results. The J_{k2} value is approximately 78 % of the J_{k1} or J_{k3} values, because K_f is

used in (2). Thus, J_k can be accurately calculated using (1) and (8) and can be used as a reference value in engineering design. As K_f is an empirical value, which is difficult to accurately determine under different conditions, this parameter is not considered further in this paper.

III. CALCULATION OF CONDUCTOR TEMPERATURE AND CURRENT CHANGE

A. Calculation of Conductor Temperature

Method 1: Adiabatic process

Equation (9) can be derived from (1) as follows

$$\theta_k = \frac{(1 + a\theta_0)e^{\frac{J_k^2 \rho_0 \alpha t_k}{rc}} - 1}{a}. \quad (9)$$

We consider a copper conductor as an example. From (9), the current density J_k changes from 0 to 300 A/mm²; the current times are t_k is 0.25 s, 0.5 s, and 1 s, respectively; and the corresponding θ_k curves are drawn in Fig. 1.

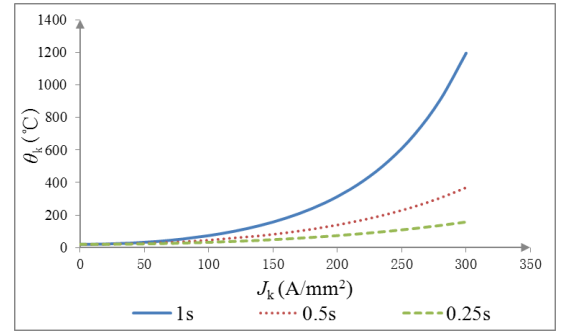


Fig. 1. Current density and conductor temperature curves.

Figure 1 shows that for the same J_k and different t_k values, θ_k grows rapidly with time period; for the same θ_k , J_k increases as t_k decreases.

Method 2: Wiedemann-Franz law

In a metal, resistivity ρ and thermal conductivity λ depend only on absolute temperature T as follows

$$\lambda \rho = LT. \quad (10)$$

The conductor temperature (11) can be calculated using (1) and (10) as follows

$$\theta_k = (273 + \theta_0)e^{\frac{J_k^2 L t_k}{c \lambda r}} - 273. \quad (11)$$

To determine whether (9) is consistent with (11), we consider the following example.

Example 2. A copper conductor is tested at an AC voltage of 230 V. We set $I_k = 1.23$ kA, $t_k = 1$ s, $\theta_0 = 20$ °C, $c = 0.39 \times 10^3$ J/(kg · °C), $r = 8.9 \times 10^3$ kg/m³, $\rho_0 = 1.67 \times 10^{-8}$ Ω · m, $\theta_k = 300$ °C, and $\alpha = 0.0039$ (1/°C).

Using (1), $J_k = 193.1$ A/mm², and $S = 6.37$ mm².

For a cross-sectional area of 10 mm² for a single core PVC copper wire, the current density $J_{k1} = 123$ A/mm².

At $t_k = 1$ s, the temperature at the end of the conductor is calculated using (9):

$$- \theta_{k1} = 110.7^\circ\text{C}.$$

At $t_k = 1$ s, the conductor end temperature is calculated

using (11) as follows: $\theta_{k2} = (273 + \theta_0) e^{\frac{J_k^2 L t_k}{c \lambda r}} - 273 = 107.3^\circ\text{C}$.

Comparing θ_{k1} and θ_{k2} shows that (9) and (11) produce almost the same result. Neglecting parameter selection and calculation error, θ_{k1} and θ_{k2} are equal. Therefore, the same results are obtained by the two different methods, proving that (9) can be used to correctly calculate θ_k .

B. Current Change Calculation

The resistance of a conductor varies with temperature according to (12)

$$R = \rho_0(1 + \alpha\theta) \frac{l}{S}. \quad (12)$$

An initial resistance of R_0 and an end resistance of R_k can be expressed as follows:

$$R_0 = \rho_0(1 + \theta_0\alpha) \frac{l}{S}, \quad (13)$$

$$R_k = \rho_0(1 + \theta_k\alpha) \frac{l}{S}. \quad (14)$$

The ratio between these two resistances is as follows

$$R_k/R_0 = (1 + \theta_k\alpha)/(1 + \theta_0\alpha) = e^{\frac{J_k^2 \rho_0 \alpha t_k}{rc}}. \quad (15)$$

It is assumed that the voltage does not change before and after the test. Then, the ratio of the currents before and after the test is as follows

$$I_k/I_0 = (1 + \theta_0\alpha)/(1 + \theta_k\alpha) = 1/e^{\frac{J_k^2 \rho_0 \alpha t_k}{rc}}. \quad (16)$$

We consider a copper conductor as an example. The current density J_k changes from 0 to 300 A/mm²; the current times t_k are 0.25 s, 0.5 s, and 1 s, respectively; and the curves of R_k/R_0 and I_k/I_0 are shown in Fig. 2.

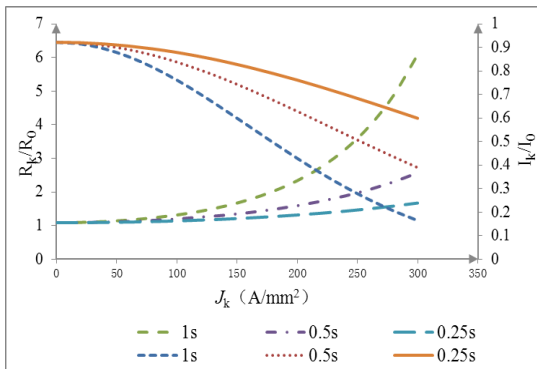


Fig. 2. Comparison of curves of current density, resistance ratio, and current ratio.

Figure 2 shows that the resistance ratio and the current ratio are directly affected by the current density and the current time. As the current density and the current time decrease, there are smaller changes in the resistance ratio and

the current ratio. As the current density and the current time increase, there is a larger variation in the resistance ratio and the current ratio.

C. Current Change Model I

We use the variation in the current ratio in Fig. 2 to develop a current change model based on the following assumptions.

- Assumption 1. The physical form of a metal conductor does not change as θ_k changes.
- Assumption 2. The thermal resistance does not change over the time of the short-circuit.
- Assumption 3. The current change is simply linear.

The current change model I based on these assumptions is given by (17) and plotted in Fig. 3.

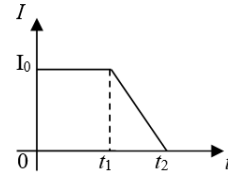


Fig. 3. Current change model I.

During the period from 0 to t_1 , the conductor temperature does not change with time due to thermal inertia; the conductor resistance and the current remains almost the approximately constant. During the period from t_1 to t_2 , the conductor temperature increases and the conductor resistance increases, so the current decreases linearly. The time t_1 and the change ratio from t_1 to t_2 are determined by the current density. This process is described in (17)

$$I = \begin{cases} I_0, & 0 \leq t \leq t_1, \\ I_0 - kt, & t_1 \leq t \leq t_2, \end{cases} \quad (17)$$

where I_0 represents the initial test current value and k represents the current gradient. The value of k depends on J_k and t_k , as seen in Figs. 1 and 2.

IV. SHORT-TIME WITHSTAND CURRENT TEST

A. Test System

The safety risk of the short-time withstand current test is very high, making it difficult to achieve the test conditions in a typical research laboratory. Our test is carried out in the National Laboratory of low voltage electrical components and switching control equipment, which has enough power supply capacity for the test. The test system has sufficient thermal and dynamic stability. The current waveform is collected using LDS. A simplified schematic of the test system is shown in Fig. 4, where U_s is an equivalent voltage source.

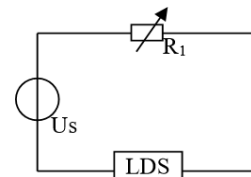


Fig. 4. Schematic of the test system.

We select special transformer; its rated capacity is 8000 kVA and short-circuit capacity is 2500 MVA, in Fig. 5. The LDS is shown in Fig. 6 and its sample frequency is 1 M/s. R_1 is an equivalent adjustable resistance, which is adjusted according to the test current, in Fig. 7.



Fig. 5. Special transformer.



Fig. 6. LDS Genesis Tower data collected system.



Fig. 7. Adjustable resistance R_1 .

Example 3. The system is tested under a DC voltage of 440 V, with $I_k = 50$ kA, $t_k = 1$ s, and $\theta_0 = 20$ °C. The test current waveform is shown in Fig. 8.

Figure 8 shows that the test system has sufficient power supply capacity for the test period. U_s remains unchanged, the thermal stability of R_1 is good, and the current remains unchanged. Therefore, the test system can meet the requirements of the following tests. The current-time curve for the test system is shown in Fig. 9.

We make the following assumptions to reflect the change in the current flowing through the metal conductor in the short-time withstand test.

– Assumption 1. The equivalent voltage source U_s and the equivalent resistance R_1 are ideal physical devices in the short-time withstand current test system.

– Assumption 2. The initial current I_0 is a constant.
– Assumption 3. The current waveform represents the actual current flowing through the equivalent resistance.

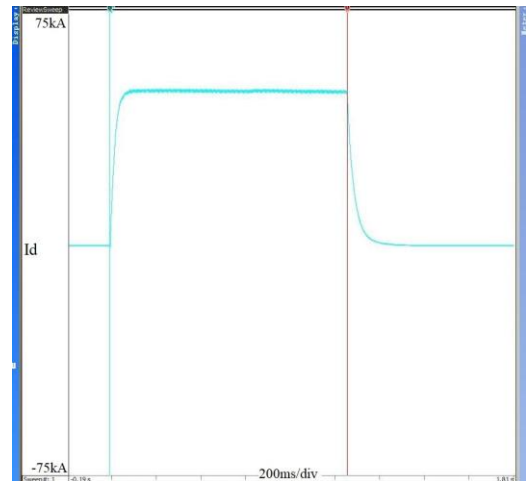


Fig. 8. 50-kA DC test current waveform.

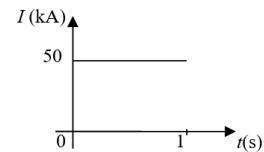


Fig. 9. Current-time curve for the test system.

B. Test Verification

The test current density is below the theoretical prediction.

Example 4. We consider 2 single core PVC copper conductor wires (denoted as #1 and #2). The wires have a length of 2 m and a cross-sectional area of 10 mm². In the test system, the single-phase AC voltage is 230 V, $I_k = 1.23$ kA, $t_k = 1$ s, and $\theta_0 = 20$ °C. A schematic of the short-time withstand current test is shown in Fig. 10. The selected current waveforms for the #1 and #2 wires are shown in Figs. 10 and 11, respectively.

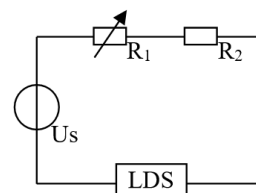


Fig. 10. Schematic of test system of #1 and #2 wires.

In Fig. 10, R_2 is the equivalent resistance of a 10 mm² wire.

The cross-sectional area is calculated using (7) as $S \geq 6.25$ mm². In this test, we select $S = 10$ mm² to meet the test requirements. The current waveforms in Fig. 11 and Fig. 12 are used to develop an approximate waveform for the test current flowing through the conductor R_2 , which is shown in Fig. 13. The following results are calculated using (15) and (16) for the equivalent resistance R_2

$$R_k/R_0 \approx 1.35 \quad I_k/I_0 \approx 0.74.$$

The current waveform can be calculated using the theory presented above and is approximated in Fig. 14.

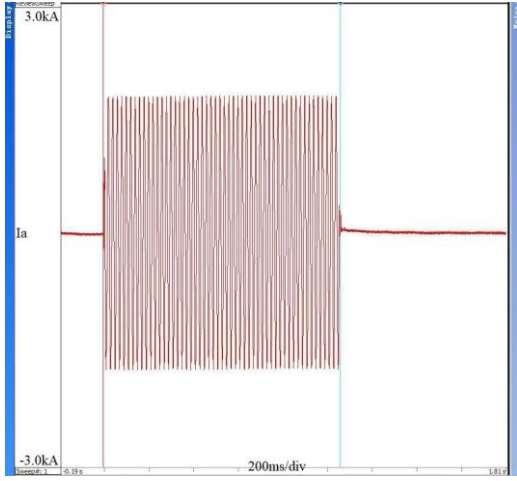


Fig. 11. Current waveform for #1 test wire.

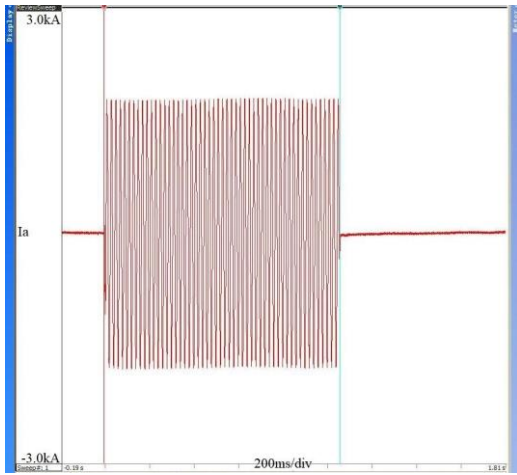


Fig. 12. Current waveform for #2 test wire.

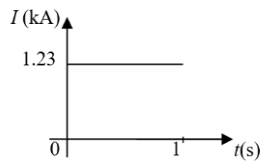


Fig. 13. Actual current waveform.

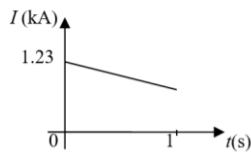


Fig. 14. Calculated current waveform from theory.

The resistance is calculated using Ohm's law as follows:

$$- R_1 + R_2 = U_s / I_k = 0.187 \Omega.$$

Then, using (12), we obtain:

$$- R_2 = 0.00334 \Omega;$$

$$- R_2 / (R_1 + R_2) \approx 0.018.$$

As $I_k / I_0 \approx 0.74$, the equivalent resistance R_2 changes the current by only $0.74 \times 0.018 = 1.33 \%$. That is, during the test, the temperature of R_2 increases, which increases the resistance and changes the measured current of the entire test system by approximately 1.33%. Comparing Figs. 13 and 14 reveals a wide gap between the test result and the theoretical prediction in the short-time withstand current test. What is the reason for this difference? The gap can be attributed to thermal inertia during the extremely short 1 s period, during

which time the current changes while the temperature remains the same: thus, the resistance does not change.

The test current density is larger than the theoretical prediction.

Example 5. We consider 2 single core PVC copper conductor wires (denoted by #3 and #4). The wires have a length of 2 m and a cross-sectional area of 2.5 mm^2 . In the test system, the single-phase AC voltage is 230 V, $I_k = 1.23 \text{ kA}$, $t_k = 1 \text{ s}$, and $\theta_0 = 20^\circ\text{C}$. A schematic of the short-time withstand current test is shown in Fig. 15. The current waveforms are shown in Figs. 16 and 17.

In Fig. 15, R_3 is the equivalent resistance of a 2.5 mm^2 wire.

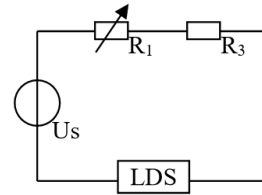


Fig. 15. Schematic of test system of #3 and #4 wires.

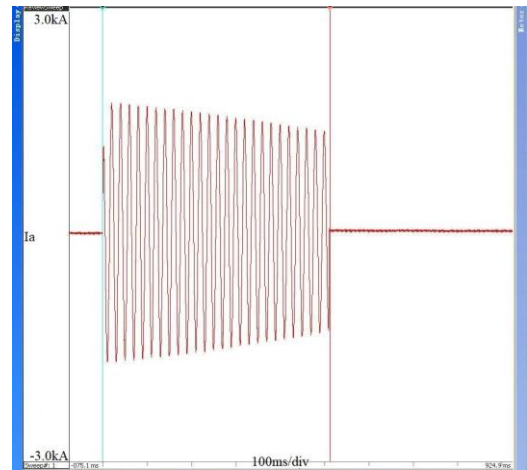


Fig. 16. Current waveform for #3 test wire.

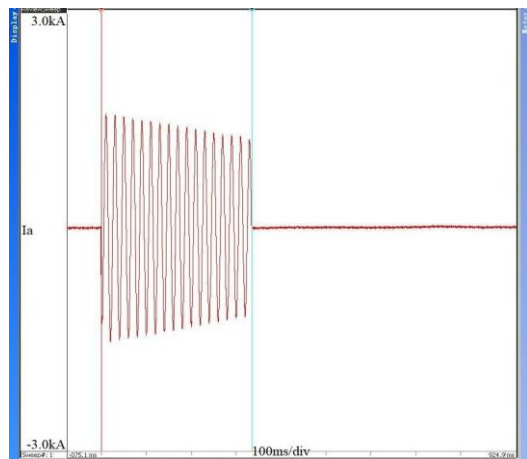


Fig. 17. Current waveform for #4 test wire.

Comparing Figs. 16 and 17 shows that the #3 wire suddenly fuses at 0.512 s, the #4 wire suddenly fuses at 0.335 s, and the polyvinyl chloride outer insulation layer of both wires is burned.

For $I_k = 1.23 \text{ kA}$ and $S = 2.5 \text{ mm}^2$, $J_k = 492 \text{ A/mm}^2$, i.e. the actual current density is larger than the theoretical prediction $J_{kI} = 193.1 \text{ A/mm}^2$.

The end temperatures of the #3 and #4 copper wires are calculated using (9) as $\theta_{k3} = 2504^\circ\text{C}$ and $\theta_{k4} = 970^\circ\text{C}$, respectively. Copper has a melting point of 1084°C and a boiling point of 2567°C . The calculated θ_{k3} is close to the boiling point of copper, and the calculated θ_{k4} is close to the melting point of copper.

The #3 and #4 wire tests show that the rapid increase in the conductor temperature results in the fusion of the conductor material and directly impacts the safe use of the electrical product under a short-circuit fault. Therefore, we must consider the temperature θ_k that is used to calculate J_k in a short-circuit fault.

Why are the results for examples 4 and 5 different? This difference can be explained in terms of the differences in current density and current time, which affect thermal inertia.

Figures 16 and 17 are used to determine the relationship between the current and the time, which is shown in Fig. 18. From $0-t_3$, the conductor temperature increases, the resistance increases, and the current decreases. At the instant t_3 , the conductor suddenly fuses and the current vanishes.

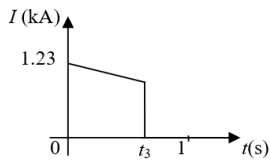


Fig. 18. Relationship between current and time for R_3 .

C. Current Change Model II

In a short-circuit fault, the effects of θ_k and J_k on the physical form of the metal conductor are used to develop the current change model II given by (18)

$$I = \begin{cases} I_0, & 0 \leq t \leq t_1, \\ I_0 - kt, & t_1 \leq t \leq t_2, \\ 0, & t_2 \leq t, \end{cases} \quad (18)$$

which is shown in Fig. 19.

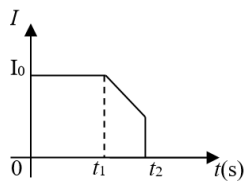


Fig. 19. Current change model II.

When J_k is below the theoretical prediction, the test waveform is shown for $0 \leq t \leq t_1$, where $t_1 = t_k$.

When J_k is greater than the theoretical prediction, the test waveform is shown for $t_1 \leq t \leq t_2$, where $t_1 = 0$, $t_2 < t_k$. As J_k is critical to the theoretical calculation, the test wave form is shown for $0 \leq t \leq t_2$, where t_1 and t_2 are uncertain and vary depending on the conditions.

V. PRODUCT DESIGN

Sustainable product design is being developed and realized more and more. Ahmad, Wong, Tseng, and Wong [25] reviewed product design tools from 2007 to 2017 and proposed a generic and comprehensive classification scheme

to improve understanding and application of these tools. Li, Lv, Tseng, and Sun [26] developed a model using an improved fuzzy reliability measure and a reliability-credibility curve, which is suitable for the coexistence of various uncertainties. Tao *et al.* [27] used a twin-driven digital method to develop a product design framework that was applied in a case study. Dey, Roy, and Saha [28] used three procurement strategies to analyze the impact of power structures and strategic inventory on the development-intensive and marginal-cost-intensive types of green products, demonstrating that green products affected the preferences of members in the supply chain.

The theoretical analysis given above and the current change model II for the short-time withstand current test lead to the following design steps for considering the thermal stability of a short-circuit fault.

- Step 1. Select reasonable values for the parameters, such as I_k , t_k , and θ_k , of a short-circuit fault, based on the product requirements and the conductor material.
- Step 2. Calculate J_k using (1).
- Step 3. Calculate the cross-sectional area of the conductor S using J_k : the local minimum cross-sectional area S_{min} should not be less than S of the electrical product.
- Step 4. Figures 1 and 2 provide theoretical reference values.
- Step 5. K_f should be considered in the design, but has an uncertain value. If $t_k \leq 1$, we can set $K_f = 1$ in an AC short-time withstand current test.

Example 6. A copper-made knife switch conductor is used as a test case. The short-time withstand current test is performed under an AC test voltage of 400 V, $I_k = 14$ kA, $t_k = 1$ s, and $\theta_0 = 20^\circ\text{C}$. The test state of the knife switch is shown in Figs. 20 and 21. The test current waveform is shown in Fig. 22.



Fig. 20. Knife switch before test.

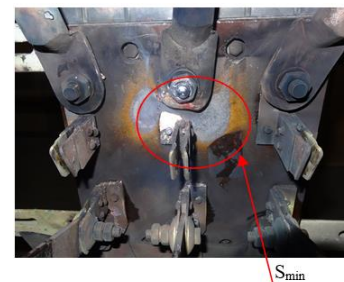


Fig. 21. Knife switch after test.

A comparison of Figs. 20 and 21 shows that the inlet terminal of phase B is fused. If the test does not terminate, phase A and phase C may also fuse. Figure 22 shows that 992 ms elapse between lines “a” and “b”, and 88 ms elapse between lines “b” and “c”.

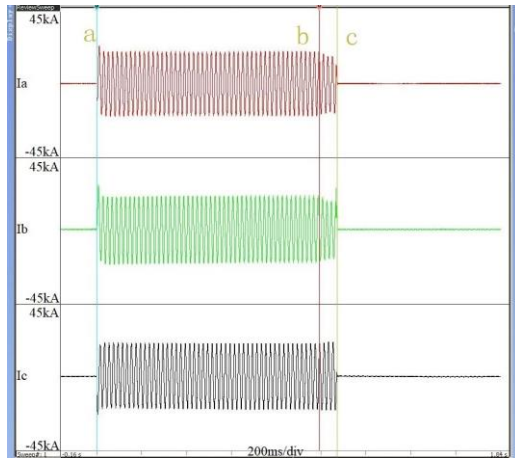


Fig. 22. Test current waveform.

The cross-sectional area of the conductor is calculated using (1) as $S = 72.5 \text{ mm}^2$. The minimum cross-sectional area measured locally S_{min} in Fig. 22 at the inlet terminal is approximately 70.6 mm^2 for phases A, B, and C. A comparison of S and S_{min} shows that the design is in a critical state. Between lines “b” and “c”, the current decreases sharply, after which phase B fuses. The power supply is turned off in time to prevent the fusion of phases A and C. The test results show that the system is in a critical state. Therefore, the cross-sectional area of the design conductor should be larger than the theoretically calculated value.

Example 7. A test is performed on a knife switch copper conductor. The short-time withstand current test is conducted under an AC test voltage of 400 V, with $I_k = 20 \text{ kA}$, $t_k = 1 \text{ s}$, and $\theta_0 = 20 \text{ }^\circ\text{C}$. The test state of the knife switch is shown in Figs. 23 and 24. The test current waveform is shown in Fig. 25.

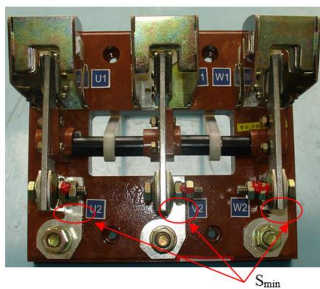


Fig. 23. Knife switch before test.

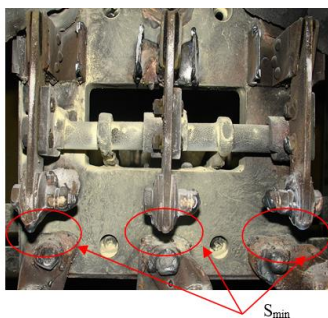


Fig. 24. Knife switch after the test.

A comparison of Figs. 23 and 24 shows that all the inlet and outlet terminals of the knife switch fuse where the cross-sectional area is smallest. Phase B first fuses at 0.056 s, and phases A and C fuse at 0.213 s with arcing.

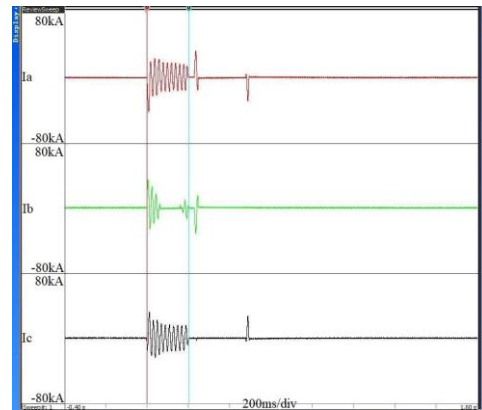


Fig. 25. Test current waveform.

The cross-sectional area of the conductor is calculated by (1) as $S = 103.6 \text{ mm}^2$: therefore, the cross-sectional area of the design conductor should be at least 120 mm^2 . The minimum sectional area is approximately 36 mm^2 , which is far less than the theoretically calculated value of 103.6 mm^2 . Thus, the cross-sectional area of the conductor S_{min} should be considered in the design, because the maximum current density flows through the minimum cross-sectional area.

VI. CONCLUSIONS

In this paper, the thermal stability of the metal conductor in short-circuit fault is analyzed. Taking the short-time withstand test of electrical products as an example, we compare three formulas for calculating current density, and we develop a theory to calculate the current density, the conductor temperature, and the current change. The theoretical results are compared and analyzed with the test results. The main conclusions are as follows:

1. The results of a short-time withstand current test exhibit deviations from theoretical predictions that are attributed to thermal inertia. Thermal inertia depends on the current density and the current time. On the basis, we develop two current change models, I and II, to describe a short-circuit fault.
2. In an AC short-time withstand current test, for $t_k \leq 1$, we select $K_f = 1$. This K_f value can meet the design requirements, thus saving copper conductor materials and costs.
3. In the design of electrical products, a reasonable metal conductor temperature is specified, the conductor cross-sectional area through theoretical calculation is obtained

At the same time, taking the short-term withstand test of electrical products as an example, based on theoretical analysis, the design steps of short-time withstand current test of electrical products have been proposed. According to these steps, the performance of electrical products to withstand short-circuit faults can be improved.

ACKNOWLEDGEMENT

The formulation of the test scheme and the measurement

and recording of the test data in this paper were completed with the strong support of the Shandong Institute of Product Quality Inspection staff (National Quality Supervision and Testing Center for low-voltage electrical components and complete sets of switchgear control equipment).

CONFLICTS OF INTEREST

The authors declare that they have no conflicts of interest.

REFERENCES

- [1] Y. Ding, Q. Zhu, Q. Le, Z. Zhang, L. Bao, and J. Cui, "Analysis of temperature distribution in the hot plate rolling of Mg alloy by experiment and finite element method", *J. Mater. Process. Technol.*, vol. 225, pp. 286–294, Nov. 2015. DOI: 10.1016/j.jmatprotec.2015.06.011.
- [2] A. Adouni and A. J. M. Cardoso, "Thermal analysis of low-power three-phase induction motors operating under voltage unbalance and inter-turn short circuit faults", *Machines*, vol. 9, no. 1, p. 2, 2021. DOI: 10.3390/machines9010002.
- [3] Z. Staliulionis, Z. Zhang, R. Pittini, M. A. E. Andersen, A. Noreika, and P. Tarvydas, "Thermal modelling and design of on-board DC-DC power converter using Finite Element Method", *Elektron. Elektrotech.*, vol. 20, no. 7, pp. 38–44, 2014. DOI: 10.5755/j01.eee.20.7.8022.
- [4] Y. Qi, M. Zafarani, B. Akin, and S. E. Fedigan, "Analysis and detection of inter-turn short-circuit fault through extended self-commissioning", *IEEE Trans. Ind. Appl.*, vol. 53, no. 3, pp. 2730–2739, May–Jun. 2017. DOI: 10.1109/TIA.2016.2626264.
- [5] A. Z. Gbégbé, B. Rouached, J. Cros, M. Bergeron, and P. Viarouge, "Damp currents simulation of large hydro-generator using combination of FEM and coupled circuits models", *IEEE Trans. Energy Convers.*, vol. 32, no. 4, pp. 1273–1283, Dec. 2017. DOI: 10.1109/TEC.2017.2719120.
- [6] R. Yang, R. Xiong, H. He, and Z. Chen, "A fractional-order model-based battery external short circuit fault diagnosis approach for all-climate electric vehicles application", *J. Clean Prod.*, vol. 187, pp. 950–959, Jun. 2018. DOI: 10.1016/j.jclepro.2018.03.259.
- [7] M. P. Macdonald, S. Chandrasekaran, S. Garimella, and T. F. Fuller, "Thermal runaway in a prismatic lithium ion cell triggered by a short circuit", *J. Energy Storage*, vol. 40, art. 102737, Aug. 2021. DOI: 10.1016/j.est.2021.102737.
- [8] W. Walendziuk, A. Idzkowski, J. Golebiowski, and P. Swietochowski, "Temperature influence analysis on the selected current sources stability in the static and dynamic operating states", *Elektron. Elektrotech.*, vol. 23, no. 2, pp. 40–46, 2017. DOI: 10.5755/j01.eie.23.2.17998.
- [9] A. Hossam-Eldin, A. Lotfy, M. Elgamal, and M. Ebeed, "Artificial intelligence-based short-circuit fault identifier for MT-HVDC systems", *IET Gener. Transm. Distrib.*, vol. 12, no. 10, pp. 2436–2443, May 2018. DOI: 10.1049/iet-gtd.2017.1345.
- [10] W. Rebizant, K. Solak, B. Brusilowicz, G. Benysek, A. Kempski, and J. Rusinski, "Coordination of overcurrent protection relays in networks with superconducting fault current limiters", *Int. J. Electr. Power Energy Syst.*, vol. 95, pp. 307–314, Feb. 2018. DOI: 10.1016/j.ijepes.2017.08.021.
- [11] R. Hrbac, V. Kolar, M. Bartłomiejczyk, T. Mlczak, P. Orsag, and J. Vanc, "A development of a capacitive voltage divider for high voltage measurement as part of a combined current and voltage sensor", *Elektron. Elektrotech.*, vol. 26, no. 4, pp. 25–31, 2020. DOI: 10.5755/j01.eie.26.4.25888.
- [12] D.-P. Sadik, J. Colmenares, G. Tolstoy, D. Peftitsis, M. Bakowski, J. Rabkowski, and H.-P. Nee, "Short-circuit protection circuits for silicon-carbide power transistors", *IEEE Trans. Ind. Electron.*, vol. 63, no. 4, pp. 1995–2004, Apr. 2016. DOI: 10.1109/TIE.2015.2506628.
- [13] X. Luo, Q. Xiao, Q. Wang, and Z. Sheng, "A novel method for distribution transformer short-circuit test", *JPCS*, vol. 1885, no. 4, 2021. DOI: 10.1088/1742-6596/1885/4/042055.
- [14] G. Kadhodaie, K. Sheshyekani, and M. Hamzeh, "Coupled electric-magnetic-thermal-mechanical modelling of busbars under short-circuit conditions", *IET Gener. Transm. Dis.*, vol. 10, no. 4, pp. 955–963, 2016. DOI: 10.1049/iet-gtd.2015.0706.
- [15] X. Huang, Q. Tan, L. Li, J. Li, and Z. Qian, "Winding temperature field model considering void ratio and temperature rise of a permanent-magnet synchronous motor with high current density", *IEEE T. Ind. Electron.*, vol. 64, no. 3, pp. 2168–2177, 2017. DOI: 10.1109/TIE.2016.2625242.
- [16] B. Guo, Z. Song, P. Fu, L. Jiang, M. Wang, and L. Dong, "Prediction of temperature rise in water-cooling DC busbar through coupled force and natural convection thermal-fluid analysis", *IEEE T. Plasma Sci.*, vol. 44, no. 12, pp. 3346–3352, Dec. 2016. DOI: 10.1109/TPS.2016.2572298.
- [17] *IEC60947-1: 2007 Low-voltage switchgear and controlgear - Part 1: General rules*, Geneva, Switzerland, 2007.
- [18] *IEC60947-3: 2005 Low-voltage switchgear and controlgear - Part 3: Switches, disconnectors and fuse-combination units*, Geneva, Switzerland, 2005.
- [19] Testing the Safety of High-Voltage Systems, HBM. [Online]. Available: <https://www.hbm.com/en/6640/kema-high-voltage-lab-using-hbms-ge-nesis-high-speed>
- [20] X. Abomailek, J.-R. Riba, F. Capelli, and M. Moreno-Eguilaz, "Fast electro-thermal simulation of short-circuit tests", *IET Gener. Transm. Distrib.*, vol. 11, no. 8, pp. 2124–2129, Jun. 2017. DOI: 10.1049/iet-gtd.2016.2061.
- [21] X. Y. He, "Electrical appliances", Beijing, China, China Machine Press, 2009, pp. 37–39.
- [22] G. S. Zhang, "Theoretical basis of electrical appliances", Beijing, China, China Machine Press, 1989, pp. 32–34.
- [23] *Electrical Engineering Electrical Design Manual - Electrical Primary Side*, Northwest electric power design institute, Beijing, China, China electric power press, 2013, p. 337.
- [24] *IEC 60949: 1988 Calculation of thermally permissible short-circuit currents, taking into account non-adiabatic heating effects*, CEI, 1988.
- [25] S. Ahmad, K. Y. Wong, M. L. Tseng, and W. P. Wong, "Sustainable product design and development: A review of tools, applications and research prospects", *Resour. Conserv. Recycl.*, vol. 132, pp. 49–61, May. 2018. DOI: 10.1016/j.resconrec.2018.01.020.
- [26] L.-I. Li, C.-M. Lv, M.-L. Tseng, and J. Sun, "Reliability measure model for electromechanical products under multiple types of uncertainties", *Appl. Soft. Comput.*, vol. 65, pp. 69–78, Apr. 2018. DOI: 10.1016/j.asoc.2018.01.005.
- [27] F. Tao, F. Sui, A. Liu, Q. Qi, M. Zhang, B. Song, Z. Guo, S. C.-Y. Lu, and A. Y. C. Nee, "Digital twin-driven product design framework", *Int. J. Prod. Res.*, vol. 57, no. 12, pp. 3935–3953, 2019. DOI: 10.1080/00207543.2018.1443229.
- [28] K. Dey, S. Roy, and S. Saha, "The impact of strategic inventory and procurement strategies on green product design in a two-period supply chain", *Int. J. Prod. Res.*, vol. 57, no. 7, pp. 1915–1948, Jan. 2019. DOI: 10.1080/00207543.2018.1511071.



This article is an open access article distributed under the terms and conditions of the Creative Commons Attribution 4.0 (CC BY 4.0) license (<http://creativecommons.org/licenses/by/4.0/>).